A numerical simulation of the Japan/East Sea (JES) seasonal circulation

Peter C. Chu, Jian Lan, and Hilbert Strauhs
Naval Postgraduate School, Monterey, CA 93943

Abstract

The seasonal variability of the Japan/East Sea (JES) circulation was studied numerically using the Princeton Ocean Model (POM) with horizontal resolution varying from 11.54 to 18.53 km and 15 sigma levels conforming to a relatively realistic bottom topography. The model was integrated using climatological monthly mean wind stresses, heat and salt fluxes as surface forcing and observational oceanic inflow/outflow at open boundaries. The seasonally averaged effects of isolated forcing terms are presented and analyzed from the following experiments: 1) non-linear effects removed, 2) no lateral transport at open boundary, and 3) wind effects removed. Major currents are simulated reasonably well compared to observations. The nonlinear advection does not affect the general circulation pattern evidently, but does affect the formation of the mesoscale eddies, especially the Ulleung/Tsushima Basin (UTB) eddy (all seasons) and the Japan Basin (JB) cyclonic gyre (spring). The lateral boundary forcing enhances (weakens) the JES volume transport in the summer (winter). The wind forcing is the most important factor (80%) for generating the JB cyclonic gyre. Besides, it drives the Liman Current and damps the East Korean Warm Current in the winter, and generates the UTB eddy, and eddies along the Japan Nearshore Branch (JNB) in all seasons. However, it has almost no effect on the JNB currents for all seasons.

1 Introduction

The Japan Sea, known as the East Sea in Korea, has a steep bottom topography (Fig. 1) that makes it a unique semi-enclosed ocean basin overlaid by a pronounced monsoon surface wind. The Japan/East Sea, hereafter referred to as JES, covers an area of 10^6 km^2. It has a maximum depth in excess of 3,700 m, and is isolated from open oceans except for small (narrow and shallow) straits, which connects the JES with the North Pacific through the Tsushima/Korean and Tsugaru Straits and with the Okhotsk Sea through the Soya and Tatar Straits. The JES contains three major basins called the Japan Basin (JB), Ulleng/Tsushima Basin (UTB), and Yamato Basins (YB), and a high central seamount called the Yamato Rise (YR). The JES has great scientific interest as a miniature prototype ocean. Its basin-wide circulation pattern, boundary currents, Subpolar Front (SPF), mesoscale eddy activities and deep water formation are similar to those in a large ocean.

Numerical studies on the JES circulations started in early 1980. Various types of models were used such as the multi-layer model (Sekine, 1986, 1991; Kawabe, 1982b; Yoon, 1982a,b; Seung and Nam, 1992a,b; Seung and Kim, 1995), the Modular Ocean Model (MOM) (Kim and Yoon, 1994; Holloway et al., 1995; Kim and Yoon, 1996; Yoshikawa et al., 1999), rigid-lid z-level model (Yoshikawa et al., 1999), the Miami Isopycnal Coordinate Model (MICOM) (Seung and Kim, 1993) and the Princeton Ocean Model (POM) (Mooer

Report Documentation Page

Form Approved
OMB No. 0704-0188

Public reporting burden for the collection of information is estimated to average 1 hour per response, including the time for reviewing instructions, searching existing data sources, gathering and maintaining the data needed, and completing and reviewing the collection of information. Send comments regarding this burden estimate or any other aspect of this collection of information, including suggestions for reducing this burden, to Washington Headquarters Services, Directorate for Information Operations and Reports, 1215 Jefferson Davis Highway, Suite 1204, Arlington VA 22202-4302. Respondents should be aware that notwithstanding any other provision of law, no person shall be subject to a penalty for failing to comply with a collection of information if it does not display a currently valid OMB control number.

1. REPORT DATE	2. REPORT TYPE	3. DATES COVERED
1999		**00-00-1999 to 00-00-1999**

4. TITLE AND SUBTITLE	5a. CONTRACT NUMBER
A numerical simulation of the Japan/East Sea (JES) seasonal circulation	5b. GRANT NUMBER
	5c. PROGRAM ELEMENT NUMBER
6. AUTHOR(S)	5d. PROJECT NUMBER
	5e. TASK NUMBER
	5f. WORK UNIT NUMBER
7. PERFORMING ORGANIZATION NAME(S) AND ADDRESS(ES) **Naval Postgraduate School,Monterey,CA,93943**	8. PERFORMING ORGANIZATION REPORT NUMBER
9. SPONSORING/MONITORING AGENCY NAME(S) AND ADDRESS(ES)	10. SPONSOR/MONITOR'S ACRONYM(S)
	11. SPONSOR/MONITOR'S REPORT NUMBER(S)

12. DISTRIBUTION/AVAILABILITY STATEMENT
Approved for public release; distribution unlimited

13. SUPPLEMENTARY NOTES
Sixth Symposium on Estuarine and Coastal Modeling, American Society of Civil Engineering, 94-113

14. ABSTRACT

15. SUBJECT TERMS

16. SECURITY CLASSIFICATION OF:			17. LIMITATION OF ABSTRACT	18. NUMBER OF PAGES	19a. NAME OF RESPONSIBLE PERSON
a. REPORT **unclassified**	b. ABSTRACT **unclassified**	c. THIS PAGE **unclassified**	**Same as Report (SAR)**	**20**	

and Kang, 1995; Chu et al., 1999c,d). Most of the numerical efforts are concentrated on simulating basin-wide circulation, the Tsushima Warm Current (TWC) bifurcation, and formation of the intermediate waters. However, there is lack of studies on dynamical mechanisms for the formation of seasonal variability of the JES circulation.

In this study, we use the POM to investigate driving mechanisms for the formation of the seasonal variabilities of the JES circulation including the subpolar front (SPF) meandering and eddies, the TWC bifurcation and its effect on the formation of mesoscale eddies in the UTB and the YB, and the Liman Cold Current (LCC) and its penetration into the southwestern waters along the Korean coast. The control run, forced by the climatological monthly wind stress, heat and fresh water fluxes, is designed to best simulate reality against which each experiment is compared. In the experiments, various external and internal factors are modified and the resulting circulation patterns and magnitudes compared to the control run results. Specifically, we estimate the contribution, in terms of volume transport and circulation patterns, of non-linear advection, wind forcing and lateral boundary transport to the ocean features identified in the control results. From this, we can estimate the relative importance of these factors to the seasonal variability of the JES circulation.

2 JES Current Systems

Most of the nearly homogeneous water in the deep part of the basin is called the Japan Sea Proper Water (Moriyasu, 1972) and is of low temperature and low salinity. Above the Proper Water, the TWC, dominating the surface layer, flows from the East China Sea through the Tsushima/Korean Strait and carries warm water from the south. The LCC flows in the JES from the Okhotsk Sea through the Tatar Strait, carries cold fresh water from the north, and becomes the North Korean Cold Current (NKCC) after reaching the North Korean coast (Yoon, 1982). Both currents turn eastward to flow roughly along 40°N latitude, forming the SPF between the Tsushma Warm Water and the cold and fresh water from the north (Fig. 2).

Uda (1934) was the first one to sketch the JES general circulation from limited observational data. The TWC separates north of 35°N into two branches into a western and an eastern channel (Kawabe, 1982a,b; Hase et al., 1999) and flows through the western channel, called the East Korea Warm Current (EKWC), and closely follows the Korean coast until it separates near 37°N into two branches. The eastern branch follows the SPF to the western coast of Sapporo Island, and the western branch moves northward and forms a cyclonic eddy at the Eastern Korean Bay (EKB). It flows through the eastern channel which closely follows the Japanese Coast, called the Nearshore Branch (NB) by Yoon (1982a). More accurately, we call it the Japan Nearshore Branch (JNB). The JNB is usually weaker than the EKWC. The strength of the Tsushima Current at both channels reduces with depth.

The NKCC meets the EKWC at about 38°N with some seasonal meridional migration. After separation from the coast, the NKCC and the EKWC converge and form a strong front that stretches in a west-east direction across the basin. The NKCC makes a cyclonic recirculation gyre in the north but most of the EKWC flows out through the outlets. The formation of NKCC and separation of EKWC are due to local forcing by wind and buoyancy flux (Seung, 1992). Large meanders develop along the front and are associated with warm and cold eddies. Readers may find qualitative depiction from a textbook written by Tomczak and Godfrey (1994).

Chu et al. (1999b) identified major features of the three-dimensional circulation and the volume transport from the Navy's $0.5° \times 0.5°$ global monthly climatological temperature and salinity data set using the P-vector method (Chu, 1995; Chu et al., 1998b). The

transport pattern is largely determined by the upper layer circulation and characterized by a large-scale cyclonic recirculation gyre, in which the EKWC and the JNB take part, as the inflow-outflow system, and the NKCC in the North. At a few hundred kilometers off the separation area, the EKWC makes an anticyclonic gyre. The gyre becomes stronger as the EKWC develops. On the other hand, the northern cyclonic gyre is very deep and is most significantly in the winter strengthened by the wind and buoyancy flux. The gyre, or the southward coastal current related to it, is deep enough to intrude southward beneath the EKWC most of the time. Seung also confirmed the summertime presence of counter-current beneath the JNB. North of the SPF there exists a cyclonic gyre in the JB usually called the JB gyre.

3 Seasonal Variation of Atmospheric Forcing

The Asian monsoon strongly affects the thermal structure of the JES (Chu et al., 1998a). During the winter monsoon season, a very cold northwest wind blows over the JES as a result of the Siberian High Pressure System. By late April, numerous frontally-generated events occur making late April and May highly variable in terms of wind speeds and number of clouds. During this period storms originating in Mongolia may cause strong, warm westerlies. By late May and early June, the summer surface atmospheric low pressure system begins to form over Asia. Initially this low pressure system is centered north of the Yellow Sea producing westerly winds. In late June, this low begins to migrate to the west setting up the southwest monsoon that dominates the summer months. The winds remain variable through June until Manchurian low pressure system strengthens. Despite the very active weather systems, the mean surface wind speed over the JES in summer is between 3 and 4 m/s, which is weaker than in winter. By July, however, high pressure (the Bonin High) to the south and the low pressure over Manchuria produce southerly winds carrying warm, moist air over the East China Sea/Yellow Sea. In the summer, warm air and strong downward net radiation stabilize the upper layer of the water and causes the surface mixed layer to shoal. October is the beginning of the transition back to winter conditions. The southerly winds weaken and let the sea surface slope reestablish the winter pattern.

The datasets used were the objectively analyzed fields of surface marine climatology and anomalies of fluxes of heat, momentum, and fresh water. The fields are derived from individual observations in the Comprehensive Ocean-Atmosphere Data Set (COADS) from 1945 to December 1989 and are analyzed on a 1° by 1° grid (da Silva et al., 1994).

4 The Numerical Ocean Model

4.1 Model Description

Coastal oceans and semi-enclosed seas are marked by extremely high spatial and temporal variability that challenge the existing predictive capabilities of numerical simulations. The POM is a time dependent, primitive equation circulation model on a three dimensional grid that includes realistic topography and a free surface (Blumberg and Mellor, 1987). River outflow is also not included. However, the seasonal variation in sea surface height, temperature, salinity, circulation and transport are well represented by the model. From a series of numerical experiments, the qualitative and quantitative effects of non-linearity, wind forcing and lateral boundary transport on the JES are analyzed, yielding considerable insight into the external factors affecting the region oceanography. The model results were sampled every thirty days.

The model contains $94 \times 100 \times 15$ horizontally fixed grid points. The horizontal spacing is 10' latitude and longitude (approximately 11.54 to 15.18 km in the zonal direction and 18.53 km in the latitudinal direction) and 15 vertical sigma coordinate levels are used. The model domain is from 35.0° N to 51.5° N, and from 127.0° E to 142.5° E. The bottom topography is the smoothed data from the Naval Oceanographic Office Digital Bathymetry Data Base 5 minute by 5 minute resolution (DBDB5). The horizontal diffusivities are modeled using the Smagorinsky (1963) form with the coefficient chosen to be 0.2 for this application. The bottom stress τ_b is assumed to follow a quadratic law

$$\tau_b = \rho_0 C_D |\mathbf{V}_b| \mathbf{V}_b \tag{1}$$

where ρ_0 ($= 1025$ kg/m^3) is the characteristic density of the sea water, $\mathbf{V}_b$ is the horizontal component of the bottom velocity, and C_D is the drag coefficient which was determined by the similarity theory.

4.2 Surface Forcing Functions

The atmospheric forcing for the JES application of the POM includes mechanical and thermohaline forcing. The wind forcing is depicted by

$$\rho_0 K_M (\frac{\partial u}{\partial z}, \frac{\partial v}{\partial z})_{z=0} = (\tau_{0x}, \tau_{0y}) \tag{2}$$

where (u, v) and (τ_{0x}, τ_{0y}) are the two components of the water velocity and wind stress vectors, respectively. The wind stress at each time step is interpolated from monthly mean climate wind stress from COADS (1945-1989). We interpolated the COADS wind stress of the resolution of $1° \times 1°$ onto the model grid of the resolution of 10'.

Surface thermal forcing is depicted by

$$K_H \frac{\partial \theta}{\partial z} = \alpha_1 (\frac{Q_H}{\rho C_p}) + \alpha_2 C(\theta_{OBS} - \theta) \tag{3}$$

$$K_S \frac{\partial S}{\partial z} = -\alpha_1 S(P - E) + \alpha_2 C(S_{OBS} - S) \tag{4}$$

where θ_{OBS} and S_{OBS} are the observed potential temperature and salinity, c_p is the specific heat, Q_H is the net surface heat flux (downward positive), P is the precipitation rate, and E is evaporation rate. The relaxation coefficient C is the reciprocal of the restoring time period for a unit volume of water. The parameters (α_1, α_2) are (0,1)-type switches: $\alpha_1 = 1$, $\alpha_2 = 0$, would specify only flux forcing is applied; $\alpha_1 = 0$, $\alpha_2 = 1$, would specify that only restoring type forcing is applied.

Chu (1989) pointed out the importance of using compatible surface wind and thermal boundary conditions. Chu et al. (1998c) further found that the restoring surface boundary condition does not exist anywhere in the world ocean. Therefore, in this study, the surface thermohaline forcing is determined solely by the flux forcing, that is, $\alpha_1 = 1$, $\alpha_2 = 0$ in (3)-(4). The mixing coefficients K_M, K_H, and K_S were computed using a level two-turbulence closure scheme (Mellor and Yamada, 1982).

4.3 Lateral Boundary Forcing

Closed lateral boundaries, i.e., the modeled ocean bordered by land, were defined using a free slip condition for velocity and a zero gradient condition for temperature and salinity. No advective or diffusive heat, salt or velocity fluxes occur through these boundaries.

At open boundaries, the numerical grid ends but the fluid motion is unrestricted. Uncertainty at open boundaries makes marginal sea modeling difficult. Three approaches,

Month	Jan	Feb	Mar	Apr	May	Jun	Jul	Aug	Sep	Oct	Nov	Dec
Soya	-0.32	-0.12	-0.20	-0.15	-0.20	-0.35	-0.55	-0.57	-0.57	-0.6	-0.6	-0.4
Tatar	0.2	0.2	0.2	0.2	0.2	0.2	0.2	0.2	0.2	0.2	0.2	0.2
Tsugaru	-0.68	-0.38	-0.60	-0.45	-0.60	-1.05	-1.65	-1.73	-1.73	-1.8	-1.8	-1.2
Tsushima	0.7	0.3	0.6	0.4	0.6	1.2	2.0	2.1	2.1	2.2	2.2	1.4

Table 1: Monthly variation of volume transport (Sv) at the lateral open boundaries. The positive/negative values mean inflow/outflow.

local-type, inverse-type, and nested basin/coastal modeling, are available for determining the open boundary condition (Chu et al., 1997). Here, we take the local-type approach, i.e., to use the radiative boundary condition with specified volume transport. When the water flows into the model domain, temperature and salinity at the open boundary are likewise prescribed from the Navy's climatological data. When water flows out of the domain, the radiation condition was applied,

$$\frac{\partial}{\partial t}(\theta, S) + U_n \frac{\partial}{\partial n}(\theta, S) = 0 \tag{5}$$

where the subscript is the direction normal to the boundary.

Warm water enters the JES through the Tsushima/Korean Strait with the TWC from the East China Sea, and cold water enters the JES through the Tatar Strait with the Liman Current from the Sea of Okhotsk (Uda, 1934). The water exits the JES through the Tsugaru and Soya straits. We use a more recent estimation of the monthly mean volume transport, reported by Chu et al. (1999b), through the Tsushima/Korean Strait with the annual average of 1.3 Sv, a maximum of 2.2 Sv in October, and a minimum of 0.3 Sv in February. The total inflow transport through the Tatar and Tsushima/Korean straits should be the same as the total outflow transport through the Tsugaru and Soya straits. We assume that 75% of the total inflow transport should flow out of the JES through the Tsugaru Strait, and 25% through the Soya Strait. The monthly volume transports at open boundaries are listed in Table 1.

4.4 Initial Conditions and Initialization

The model was integrated with all three components of velocity (u, v, w) initially set to zero, and with temperature and salinity specified by interpolating climatology data to each model grid point. The model year consists of 360 days (30 days per month), day 361 corresponds to 1 January. It was found that 90 days were sufficient for the model kinetic energy to reach quasi-steady state under the imposed conditions. In order to first capture the winter monsoon to summer monsoon transition, the model was started from 30 October, and run to 30 January next year for spin-up. After that day (30 January), the model was run another three years for each experiment. The monthly mean data are used for comparison.

4.5 Mode Splitting

For computational efficiency, the mode splitting technique (Blumberg and Mellor, 1987) is applied with a barotropic time step of 25 seconds, based on the Courant-Friederichs-Levy (1928) computational stability (CFL) condition and the external wave speed; and a baroclinic time step of 900 seconds, based on the CFL condition and the internal wave speed.

4.6 Volume Transport Streamfunction

To investigate the JES circulation as a whole, we integrate the velocity vertically from the surface ($z = 0$) to the bottom ($z = -h$)

$$(U, V) = \int_{-h}^{0} (u, v) dz \tag{6}$$

Due to the continuity the volume transport stream function (Ψ) is defined by

$$U = -\frac{\partial \Psi}{\partial y}, \quad V = \frac{\partial \Psi}{\partial x} \tag{7}$$

and satisfies the Poisson equation

$$(\frac{\partial^2}{\partial x^2} + \frac{\partial^2}{\partial y^2})\Psi = \frac{\partial V}{\partial x} - \frac{\partial U}{\partial y} \tag{8}$$

For each time instance, we solve the two-dimensional Poisson equation (10) with the given boundary conditions, that is, zero transport at the rigid boundaries and known transport at the open boundaries (see Table 1).

5 The Simulated Circulation (Control Run)

5.1 General Description

The simulated surface velocity field (Fig. 3) coincides with the earlier description of the JES circulation presented in Section 2. The TWC separates at the Tsushima/Korea Strait into western and eastern branches. Flow through the western channel (i.e., EKWC) closely follows the Korean coast until it separates near 38°N into two branches. The eastern branch follows the SPF to the western coast of Sapporo Island, and the western branch, moves northward and forms a cyclonic eddy at the Eastern Korean Bay (EKB). Flow through the eastern channel (i.e., JNB) is a little weaker than through the western channel. The simulated LCC carries fresh and cold water along the Russian coast and becomes the NKCC at the North Korean coast. The simulated NKCC meets the EKWC at about 38°N. After separation from the coast, the NKCC and the EKWC converge to a strong front that runs in the west-east direction across the basin.

5.2 JB Cyclonic Gyre

A large-scale cyclonic recirculation gyre over the JB is simulated with a strong seasonal variation. This gyre is easily identified by the volume transport streamfunction (Fig. 4). The JB gyre is the strongest and recirculates 8 Sv in the winter. It weakens and retreats northward in the spring and summer. In the fall, the cyclonic JB gyre disappears and weak anticyclonic eddies appears.

5.3 LCC

The LCC is a southwestward current following along the Russian coast. It bifurcates into two branches near the east Russian bight (134°E, 42°N): the western branch flows along the Russian-Korean coast and becomes the NKCC. The eastern branch flows southeastward, then turns eastward at 41.5°N, and becomes the south flank of the JB gyre. The LCC has a strong seasonal variation with the maximum speed in the winter (Fig. 3a) and the minimum speed in the summer (Fig. 3c).

5.4 EKWC

EKWC, western branch of TC north of the Tsushima/Korea Strait, acts as a western boundary current and has a strong seasonal variability. At 37°N, the EKWC v-velocity component, which is practically the direction of the current on that position, varies from 0.30 m/s in winter to 0.42 m/s in summer (Fig. 5). The width of EKWC is around 60 km all year round. However, the depth is around 1,400 m in the summer and 800 m in the winter.

5.5 EKWC - NKCC Confluence

The (northward) overshooting of the EKWC near the Korean Bight at 37.5°N is stronger in the winter than in the summer (Fig. 3). The overshot EKWC leaves the Korean coast and moves northward. It converges with the southward flowing NKCC, at 39°N, 130°E, and forms a current meandering toward the east along the SPF. We may call it the SPF Current (PFC).

5.6 JNB

JNB, the eastern branch of TC north of the Tsushima/Korea Strait at 135°E, has a maximum eastward component of 0.18 m/s in the winter (Fig. 6). A counter current beneath it is simulated with a westward component of 0.09 m/s. In the summer, the counter current remains almost unchanged, but the JNB increases to 0.21 m/s (Fig. 6).

5.7 UTB Eddy

The western branch of the warm TC (i.e., EKWC) moves northward along the southern part of Korean coast and separates from the coast after approaching the East Korean Bay (EKB). It keeps its northward motion until meeting the NKCC near 40°N, meanders southeastward, and forms a warm-core anticyclonic eddy (Fig. 3). The simulated anticyclonic UTB eddy is strongest in the summer (Fig. 3c). The center is located at 38.5°N 130°E. The size of the eddy is around 150 km. The tangential velocity is around 0.4 m/s.

6 Driving Mechanisms

We analyzed the results of the four experiments to identify the driving mechanisms for the JES circulation.

6.1 Effects of Nonlinearity (Run 1 - Run 2)

In the first sensitivity study, the nonlinear advection terms were removed from the dynamic equations. Otherwise, the same parameters as the control run were used. The figures and analysis were performed after computing the difference between control and non non-linear terms runs. The differential surface vector velocities (Fig. 7) do not show evidence for general circulation patterns except a couple of mesoscale eddies, and especially the UTB eddy, which indicates that the non-linearity does not change the general circulation pattern except for the UTB anticyclonic eddy. However, our computation shows that the non-linearity causes a noticeable change in the volume transport.

6.2 Wind-Induced Circulation (Run 1 -Run 3)

Compared to the surface velocity vector map for the control run (Fig. 3), the surface differential current vectors $\Delta \mathbf{V}$ (Fig. 8) clearly show the wind effects on the JES circulation: (a) driving the LCC in the winter, (b) damping the EKWC especially in the winter,

(c) generating the UTB eddy in all the seasons, and (d) generating eddies along the JNB. The wind has almost no effect on the occurrence of the JNB for all seasons.

The winter monsoon winds blow from the northwest to the southeast over the JES surface and drives the Ekman flow in the upper ocean to the right of the wind direction. Such a surface current moves southward at the western coast of the JES and strengthens the LCC and weakens the EKWC. The summer monsoon winds blow from the south and southeast to the northwest with much smaller speeds. Thus, the summer wind effects on reducing LCC and strengthening EKWC are quite weak.

The winds drive mesoscale eddies especially near UTB and along the west coast of Honshu. The surface UTB eddy, occurring on the differential velocity vector map (Fig. 8), has the similar swirl velocity (anticyclonic) with same order of magnitudes (maximum value of 0.7 m/s) as the control run (Fig. 3). This means that the wind effect is in fact a key factor for generating the UTB anticyclonic eddy. Furthermore, there is no evident current along the west coast of Honshu on the $\Delta \mathbf{V}$ map (Fig. 8), indicating that wind forcing is not a major factor for maintaining JNB.

6.3 Inflow/Outflow Induced Circulation (Run 1 - Run 4)

The third sensitivity study used the control run equations and forcing but closed all open lateral boundaries, preventing the transport of mass, heat or salinity through the Tsushima, Tsugaru, Soya, and Tatar Straits. With inflow or outflow, the JES vertically integrated circulation pattern is more pronounced in the summer than in the winter. This is because Ψ (control - no transport) pattern (Fig. 9) is quite similar to Ψ_C (control run) (Fig. 4) in the summer than in the winter. Increased circulation in the summer by the lateral transport generally leads to greater horizontal and vertical variabilities of the current structure. In the winter, Ψ has positive values (2 Sv), and Ψ_C has negative values in JB. This suggests that the lateral transport reduces the JB cyclonic gyre by 2 Sv in the winter.

7 Conclusions

(1) The JES circulation was simulated in this study by the POM model under the seasonal surface flux forcing. The northern JES (i.e., the Japan Basin) is occupied by a cyclonic gyre (called the JB gyre) and the southern JES is characterized as a multi-eddy structure. The volume transport streamfunction has a double-gyre structure with negative values (cyclonic) in the northern JES and positive values (anticyclonic) in the southern JES. The simulated JB gyre is the strongest and recirculates 8 Sv in the winter. It weakens and retreats northward in the spring and summer. In the fall, the cyclonic JB gyre disappears and weak multi-anticyclonic eddies appear.

(2) The current systems such as the LCC, EKWC, NKCC, and JNB are simulated reasonably well. The simulated LCC has a maximum southward component (0.21 m/s), occurring near the surface in the winter with a width of 100 km and extending to a depth of 800 m. It weakens to a minimum of 0.15 m/s in the summer and fall, and shrinks in size to a width of 60 km and depth of 400 m.

The simulated EKWC varies from 0.42 m/s (summer) to 0.30 m/s (winter). The width of the EKWC is around 60 km all year round. However, the depth is around 1,400 m in the summer and 800 m in the winter. The (northward) overshot EKWC leaves the Korean coast moving northward and converges with the southward flowing NKCC, at 40°N, 130°E, and forms a current meandering toward east along the SPF.

The simulated JNB has a maximum eastward component of 0.24 m/s in the winter and weakens to 0.09 m/s in the summer. This is consistent with the earlier observational

study. The effect of coastal geometry, such as the Noto Peninsula on the JNB, is also simulated.

The simulated UTB warm-core anticyclonic eddy has a western branch of the TWC (i.e., EKWC) which moves northward along the southern part of the Korean coast and separates from the coast after approaching the East Korean Bay. It keeps its northward motion until meeting the NKCC near 40° N, meanders southeastward, and forms a warm-core anticyclonic eddy. This eddy is strongest in the summer and its center is located at 38.5° N 130° E. The size of the eddy is around 150 km. The tangential velocity is around 0.4 m/s.

(3) The nonlinear advection does not affect the general circulation pattern evidently, but does affect the formation of the mesoscale eddies, and especially the UTB eddy (all seasons) and the JB cyclonic gyre (spring).

(4) The model wind effects on the JES circulation are more pervasive than those of non-linear dynamic effects. The winter winds cause a strong basin-wide JES cyclonic gyre with 8 Sv recirculation in the northern JES and the summer winds drive a weak nearly basin-wide JES anticyclonic gyre. Thus, the wind forcing is the most important fact (80%) for the generation of the JB cyclonic gyre. Besides, the winds also influence the surface circulation such as driving the LCC (winter), damping the EKWC (winter), generating the UTB eddy (all seasons), and generating eddies along the JNB (all seasons). The wind has almost no effect on the occurrence of the JNB for all seasons.

(5) The model boundary-forcing enhances (weakens) the JES volume transport in the summer (winter). It has very weak effects on the occurrence of the LCC except in the winter, when the boundary-forcing accounts for 30% of the LCC at 46° N. It weakens the JB cyclonic gyre by 2 Sv (25%) in the winter. Besides, the boundary forcing also influences the surface circulation such as driving the UTB eddy in all the seasons (50% in the winter), generating the EKWC (50-100%) in the winter and 21% in the summer), and generating the JNB and eddies along the JNB.

(6) Future studies should concentrate on less simplistic scenarios. Realistic lateral transport should be included and the use of extrapolated climatological winds needs to be upgraded to incorporate synoptic winds to improve realism. Finally, the assumption of quasi-linearity that allowed us to use simple differences to quantify the effect of external forcing needs to be rigorously tested. It is very important to develop a thorough methodology to perform sensitivity studies under the highly non-linear conditions that may exist in the littoral environment.

8 Acknowledgments

The authors wish to thank George Mellor and Tal Ezer of the Princeton University for most kindly proving us with a copy of the POM code and to thank Chenwu Fan and Yuchun Chen for programming assistance. This work was funded by the Office of Naval Research NOMP Program, the Naval Oceanographic Office, and the Naval Postgraduate School.

References

[1] Blumberg, A., and G. Mellor, 1987: A description of a three dimensional coastal ocean circulation model. Three-Dimensional Coastal Ocean Models, edited by N.S. Heaps. *Amer. Geophys. Union*, Washington D.C., 1-16.

[2]Cai, W.J., and P.C. Chu, 1998: A thermal oscillation under a restorative forcing. *Q. J. R. Meteorol. Soc.*, **124**, 793-809.

[3]Chu, P.C., 1989: Relationship between thermally forced surface wind and sea surface temperature gradient. *Pure Appl. Geophys.*, **130**, 31-45.

[4]Chu, P.C., 1995: P-vector method for determining absolute velocity from hydrographic data. *Marine Tech. Soc. J.*, **29**(3), 3-14.

[5]Chu, P.C., C.W. Fan, and L.L. Ehret, 1997: Determination of open boundary conditions from interior observational data. *J. Atmos. Oceanic Tech.*, **14**, 723-734.

[6]Chu, P.C., Y.C. Chen, S.H. Lu, 1998a: Temporal and spatial variabilities of Japan Sea surface temperature and atmospheric forcings. *J. Oceanogr.*, **54**, 273-284.

[7]Chu, P.C., C.W. Fan, and W.J. Cai, 1998b: P-vector inverse method evaluated using the Modular Ocean Model (MOM). *J. Oceanogr.*, **54**, 185-198.

[8]Chu, P.C., Y.C. Chen, and S.H. Lu, 1998c: On Haney-type surface thermal boundary conditions for ocean circulation models. *J. Phys. Oceanogr.*, **28**, 890-901.

[9]Chu, P.C., S.H. Lu, and Y.C. Chen, 1999a: A coastal atmosphere-ocean coupled system (CAOCS) evaluated by an airborne expandable bathythermograph survey in the South China Sea, May 1995. *J. Oceanogr.*, **55**, 543-558.

[10]Chu, P.C., J. Lan, and C.W. Fan, 1999b: Japan/East Sea (JES) seasonal circulation and thermohaline variabilities, Part 1, Climatology. *J. Phys. Oceanogr.*, submitted.

[11]Chu, P.C., S.H. Lu, and Y.C. Chen, 1999c: Circulation and thermohaline structures of the Japan/east Sea (JES) and adjacent seas simulated by a nested basin/coastal model, p.108-111, *Proc. CREAMS'99*, Fukuoka, Japan, Jan. 26-28, 1999.

[12]Chu P. C., Y. Chen, S. Lu, 1999d: Japan/East Sea (JES) SPF Meandering and Eddy Shedding in May 1995, p 11-13, *Proc. CREAMS'99*, Fukuoka, Japan, Jan. 26-28, 1999.

[13]Courant, R., K.O. Friedrichs, and H. Levy, 1928: Uber die partiellen differenzengleichungen der mathematischen physik. *Math. Annalen*, **100**, 32-74.

[14]Hase, H., J.-H. Yoon, W. Koterayama, 1999: The Branching of the Tsushima Warm Current along the Japanese coast., p 19-22, *Proc. CREAMS'99*, Fukuoka, Japan, Jan. 26-28, 1999.

[15]da Silva, A.M., C.C. Young, and S. Levitus, 1994: Atlas of Surface Marine Data 1994. *Tech. Rep. Geosci.*, 94, University of Wisconsin-Milwakee, 83pp.

[16]Hirose, N., C.H. Kim, and J.H. Yoon, 1996: Heat budget in the Japan Sea. *J. Oceanogr., Soc. Jpn.*, **52**, 553-574.

[17]Holloway, G.T. Sou and M. Eby, 1995. Dynamics of circulation of the Japan Sea. *J. Mar. Res.*, **53**, 539-569.

[18]Kawabe, M., 1982a: Branching of the Tsushima Current in the Japan Sea, Part I: Data analysis. *J. Oceanogr. Soc.*, **38**, 95 - 107.

[19]Kawabe, M., 1982b: Branching of the Tsushima Current in the Japan Sea, Part II: Numerical experiment. *J. Oceanogr. Soc.*, **38**, 183 - 192.

[20]Kim, C.-H. and J.-H. Yoon, 1994: A numerical study on the seasonal variation of the Tsushima Warm Current along the coast of Japan. Proceedings of the CREAMS Third Workshop. Seoul, Korea, pp. 73-79.

[21]Kim. C.-H. and J.-H. Yoon, 1996: Modeling of the wind-driven circulation in the Japan Sea using a reduced gravity model. *J. Oceanogr.*, **52**, 359-373.

[22]Mellor. G., and T. Yamada, 1982: Development of a turbulence closure model for geophysical fluid problems. *Rev. Geophys. Space Phys.*, **20**, 851-875.

[23]Mooers. C. N.K. and H.-S. Kang (1995). Initial spin-up of a Sea of Japan numerical circulation model. In: (Eds. A.S. Alekseev and N.S. Bakhvalov) Advanced Mathematics: Computations and Applications, NCC Publisher, Novosibirsk; pp. 350-357.

[24]Ro. Y. J.. 1999. Numerical Experiments of the Meso - Scale Eddy Activities in the East (Japan) Sea. p 116-119. *Proc. CREAMS'99*, Fukuoka, Japan, Jan. 26-28, 1999.

[25]Smagorinsky, J.. General circulation experiments with the primitive equations, I. The basic experiment, *Mon. Wea. Rev.*, **91**, 99-164, 1963.

[26]Sekine, Y. , 1986: A numerical experiment on the seasonal variation of the oceanic circulation in the Japan Sea. In: Oceanography of Asian Marginal Seas (Ed., K. Takano) Elsevier Oceanography Series, 54:113-128.

[27]Sekine. Y., 1991: Wind-driven circulation in the Japan Sea and its influence on the branching of the Tsushima Current. *Prog. Oceanogr.*, **17**, 297-312.

[28]Seo. J. W.. 1998: Research on the sea surface winds and heat flux in the East Asian Marginal Seas. Ph.D Thesis, Hanyang University.

[29]Seung, Y.H., 1992: A simple model for separation of East Korean Warm Current and formation of the North Korean Cold Current. *J. Oceanol. Soc. Korea*, **27**, 189-196.

[30]Seung. Y.H. and K. Kim. 1989: On the possible role of local thermal forcing on the Japan Sea circulation. *J. Oceanol. Soc. Korea*, **24**: 1-14.

[31]Seung. Y.H., S.Y. Nam, and S.R. Lee, 1990: A combined effect of differential cooling and topography on the formation of Ulleung Warm Eddy. *Bull. Korean Fish. Soc.*, **22**, 375-384.

[32]Seung, Y.-H. and S.-Y. Nam, 1991: Effect of winter cooling of subsurface hydrographic conditions off Korean Coast in the East (Japan) Sea. In: Oceanography of Asian Marginal Seas (Ed., K. Takano) Elsevier Oceanography Series, pp. 163-178.

[33]Seung, Y.H. and S.Y. Nam, 1992a: A numerical study on the barotropic transport of the Tsushima Warm Current. *La mer*, **30**, 139-147.

[34]Seung, Y.H. and S.Y. Nam, 1992b: A two-layer model for the effect of cold water formation on the East Korean Warm Current. *Bull. Korean Fish. Soc.*, **25**, 65-72.

[35]Seung, Y.-H. and K. Kim, 1993: A numerical modeling of the East Sea circulation. *J. Oceanol. Soc. Korea*, **28**, 292-304.

[36]Seung, Y.H. and K.J. Kim, 1995: A multilayer model for dynamics of upper and intermediate layer circulation of the East Sea. *J. Oceanol. Soc. Korea*, **30**, 227-236.

[37]Tomczak, M., and J.S. Godfrey, 1994: Regional Oceanography: An Introduction. Pergamon, Tarrytown, New York, pp.180-181.

[38]Uda, M., 1934: The results of simultaneous oceanographic investigartions in the Japan Sea and its adjacent waters in May and June. *J. Imp. Fish. Exp. Sta.*, **5**, 57-190 (in Japanese).

[39]Yoon, J.-H., 1982a: Numerical experiment on the circulation in the Japan Sea, Part I. Formation of the East Korean Warm Current. *J. Oceanogr. Soc. Japan*, **38**, 43-51.

[40]Yoon, J.-H. 1982b: Numerical experiment on the circulation in the Japan Sea, Part II. Influence of seasonal variations in atmospheric conditions on the Tsushima Current. *J. Oceanogr. Soc. Japan*, **38**, 81-94.

[41]Yoon, J.-H. 1982c: Numerical experiment on the circulation in the Japan Sea Part, III. Mechanism of the Nearshore Branch of the Tsushima Current. *J. Oceanogr. Soc. Japan*, **38**, 125-130.

[42]Yoshikawa, Y., T. Awaji, and K. Akitomo, 1999: Formation and circulation processes of intermediate water in the Japan Sea. *J. Phys. Oceanogr.*, **29**, 1701-1722.

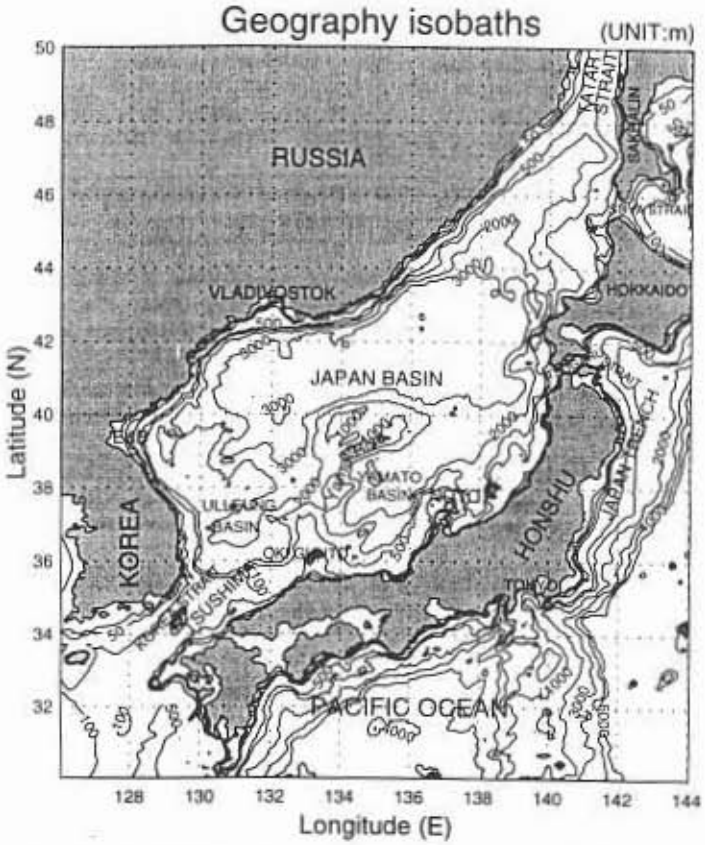

Fig. 1. Geography and isobaths showing the bathymetry (m) of the Japan/East Sea (JES).

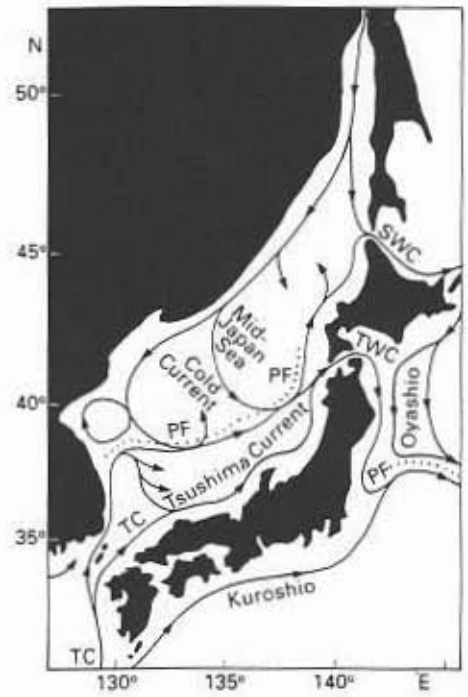

Fig. 2. Schematic map of surface current systems (after Tomczak and Godfrey, 1994).

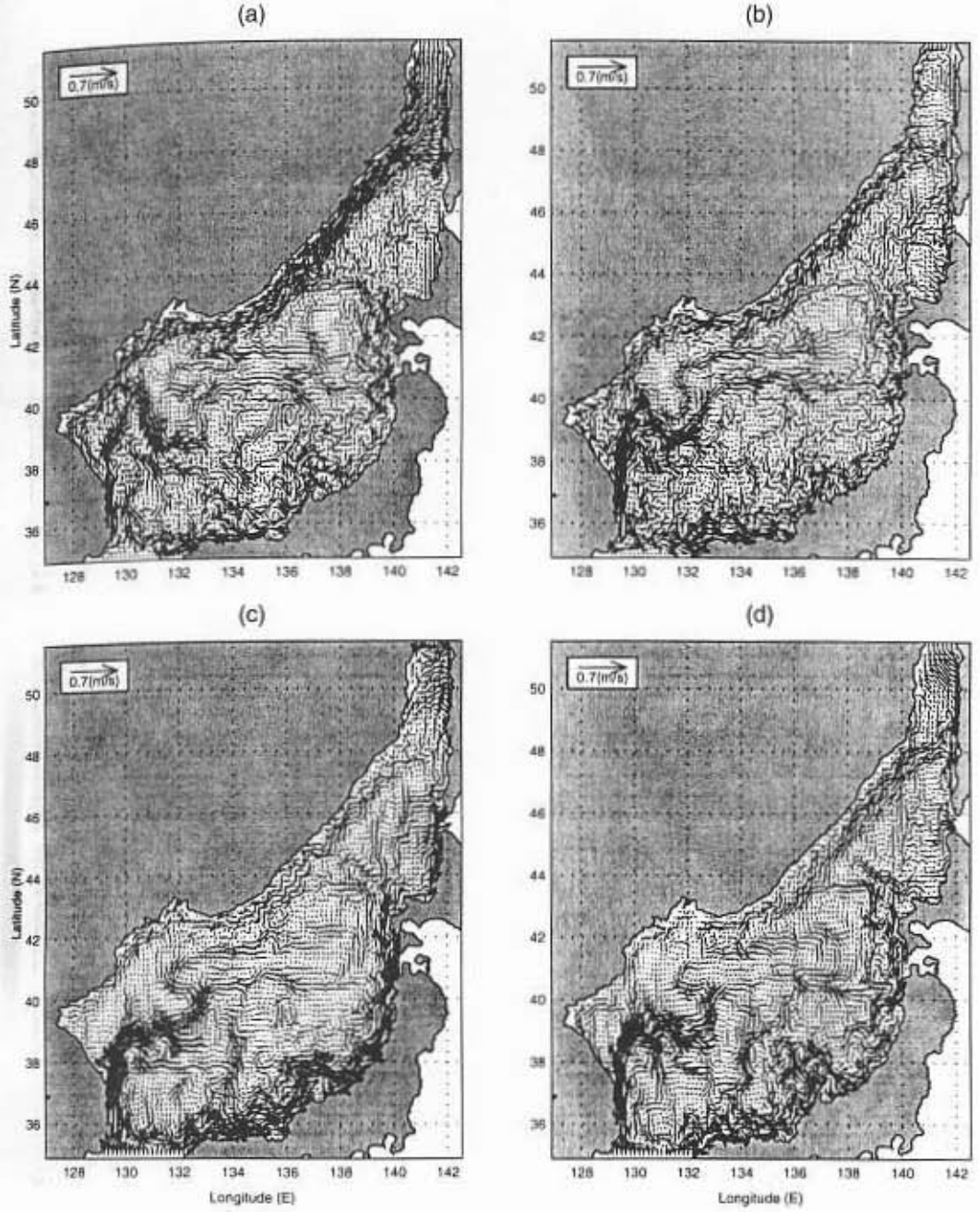

Fig. 3. Simulated surface circulation from the control run for (a) January, (b) April, (c) July and (d) October.

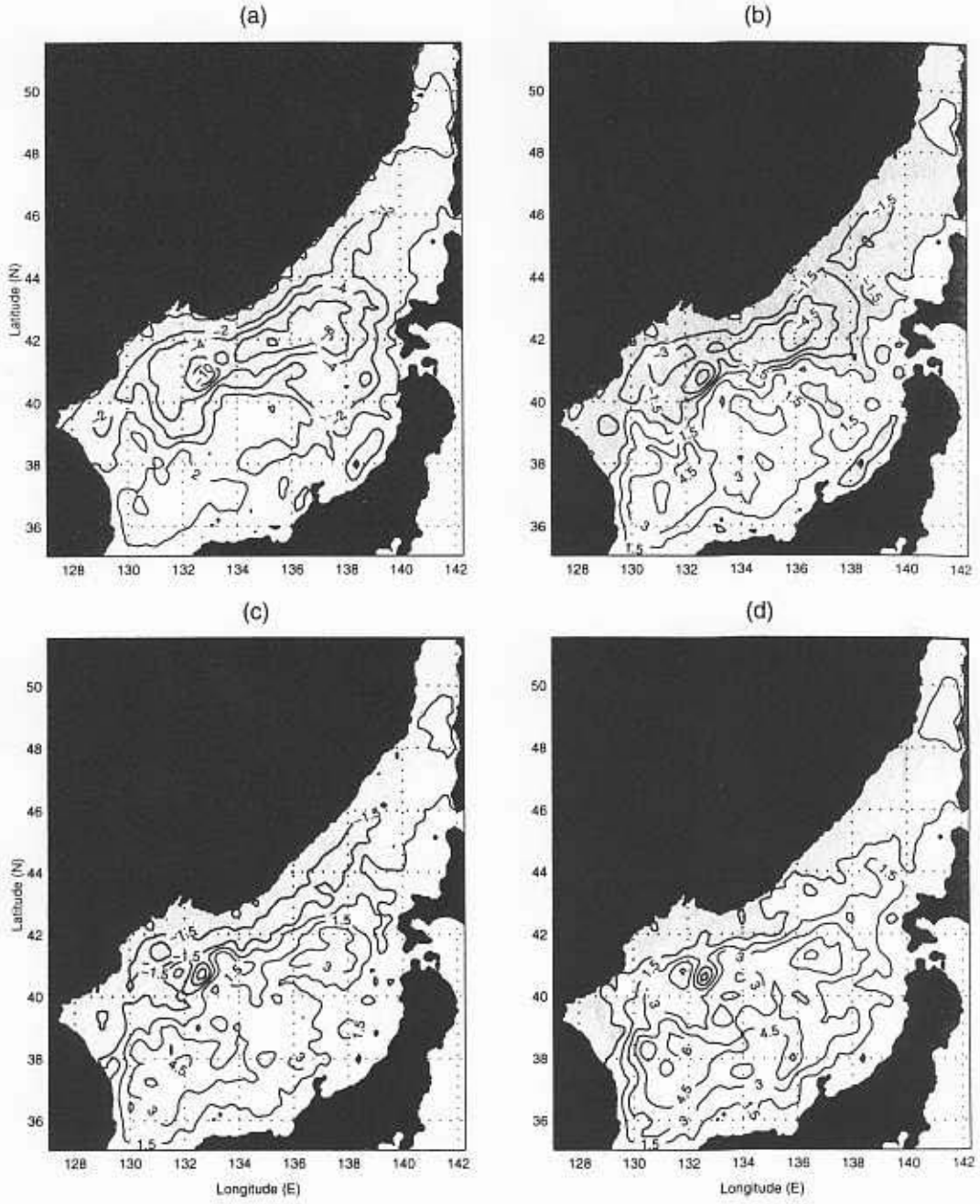

Fig. 4. Simulated volume transport (Sv) from the control run for (a) January, (b) April, (c) July and (d) October.

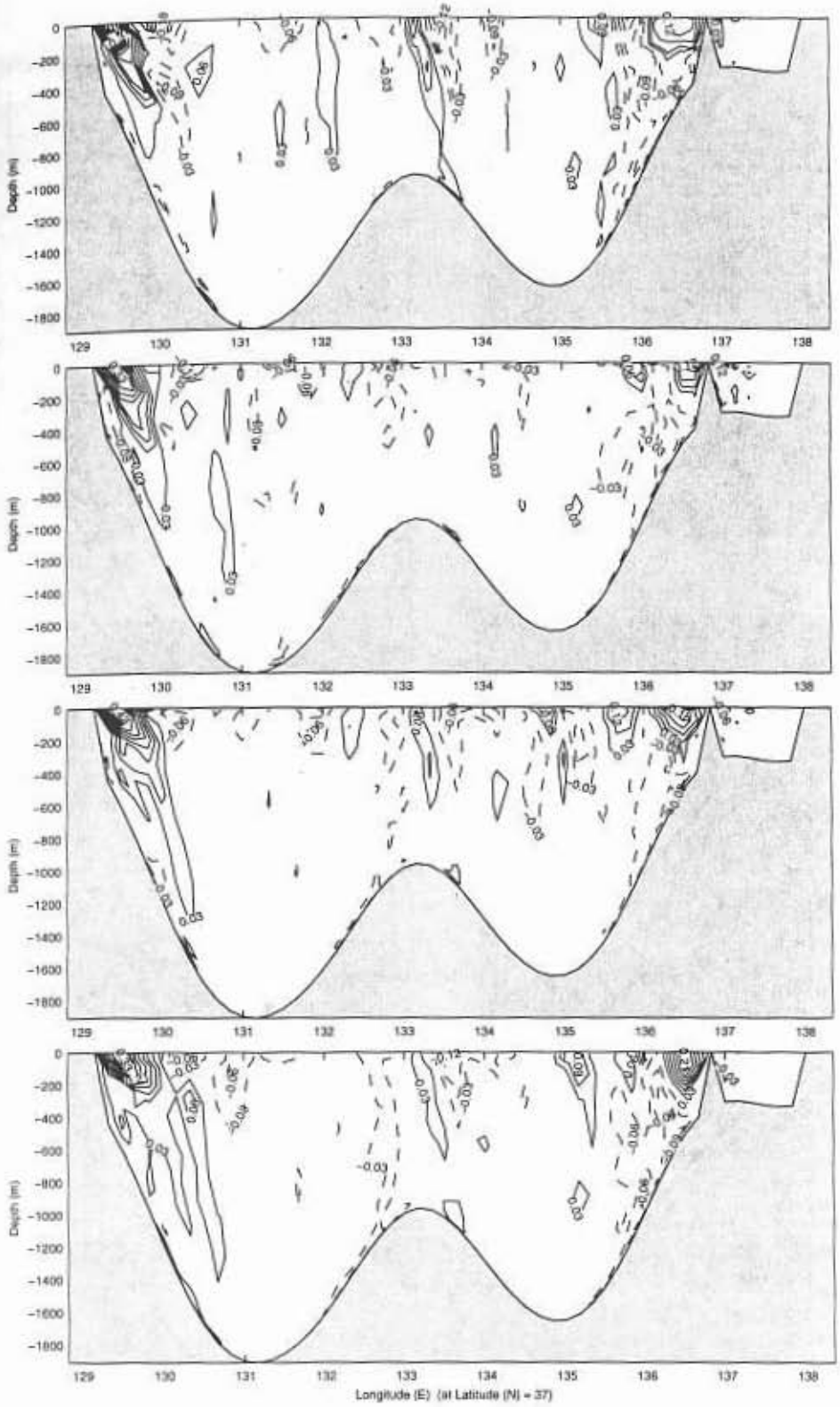

Fig. 5. Simulated zonal cross-section of v-velocity component (m/s) along 37°N from the control run for (a) January, (b) April, (c) July and (d) October.

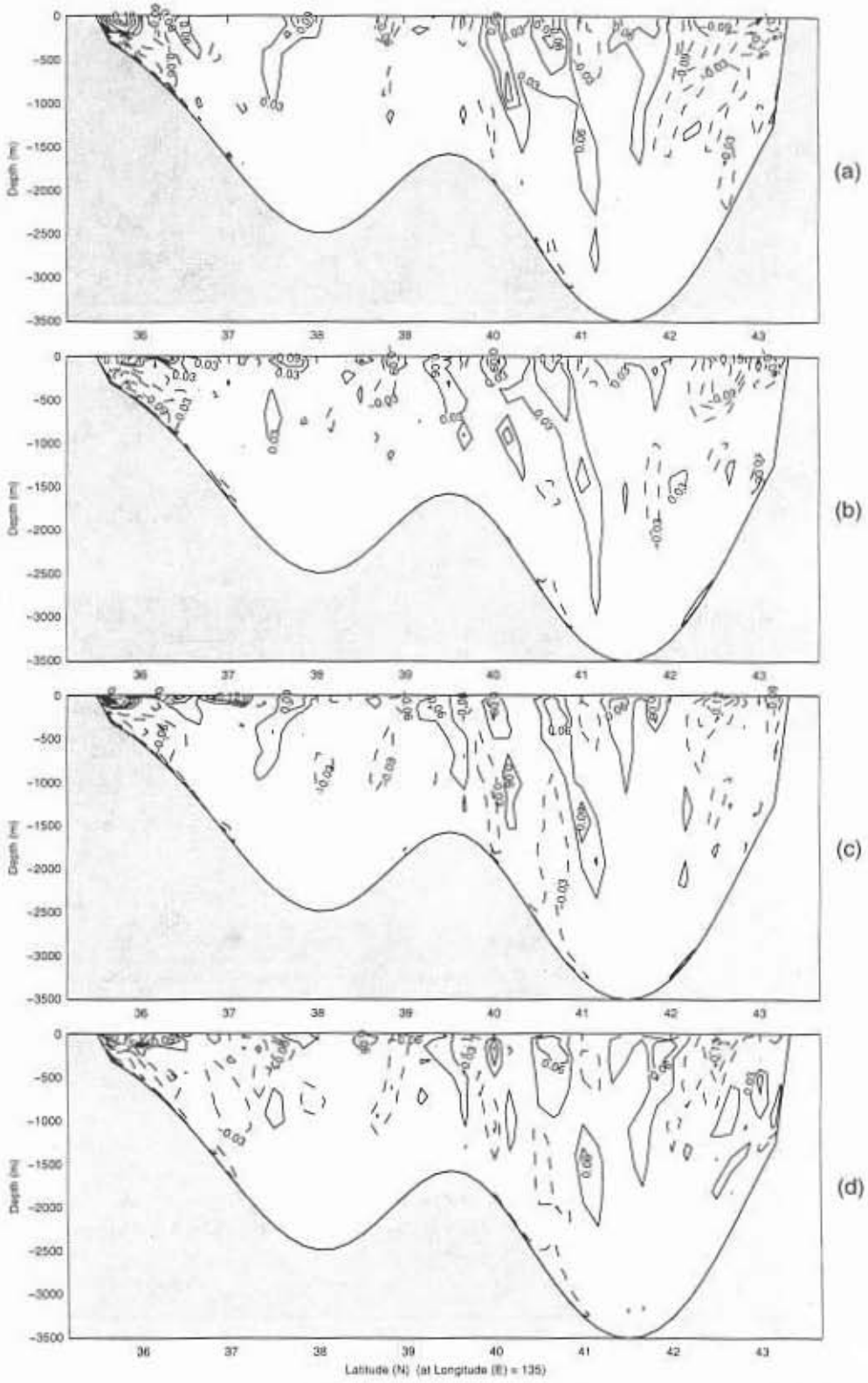

Fig. 6. Simulated latitudinal cross-section of u-velocity component (m/s) along 135°E from the control run for (a) January, (b) April, (c) July and (d) October.

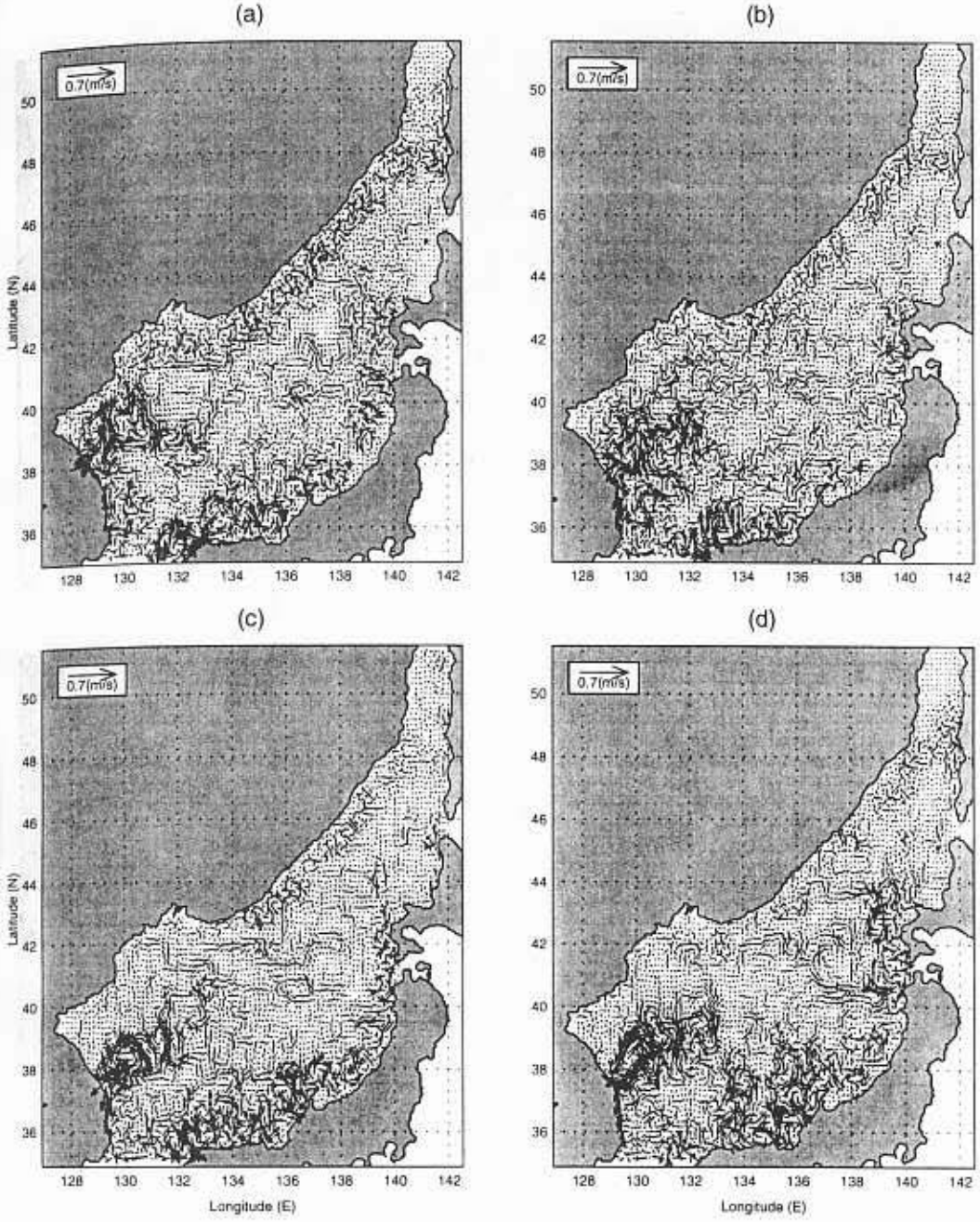

Fig. 7. Surface circulation caused by the non-linear effect: (a) January, (b) April, (c) July and (d) October.

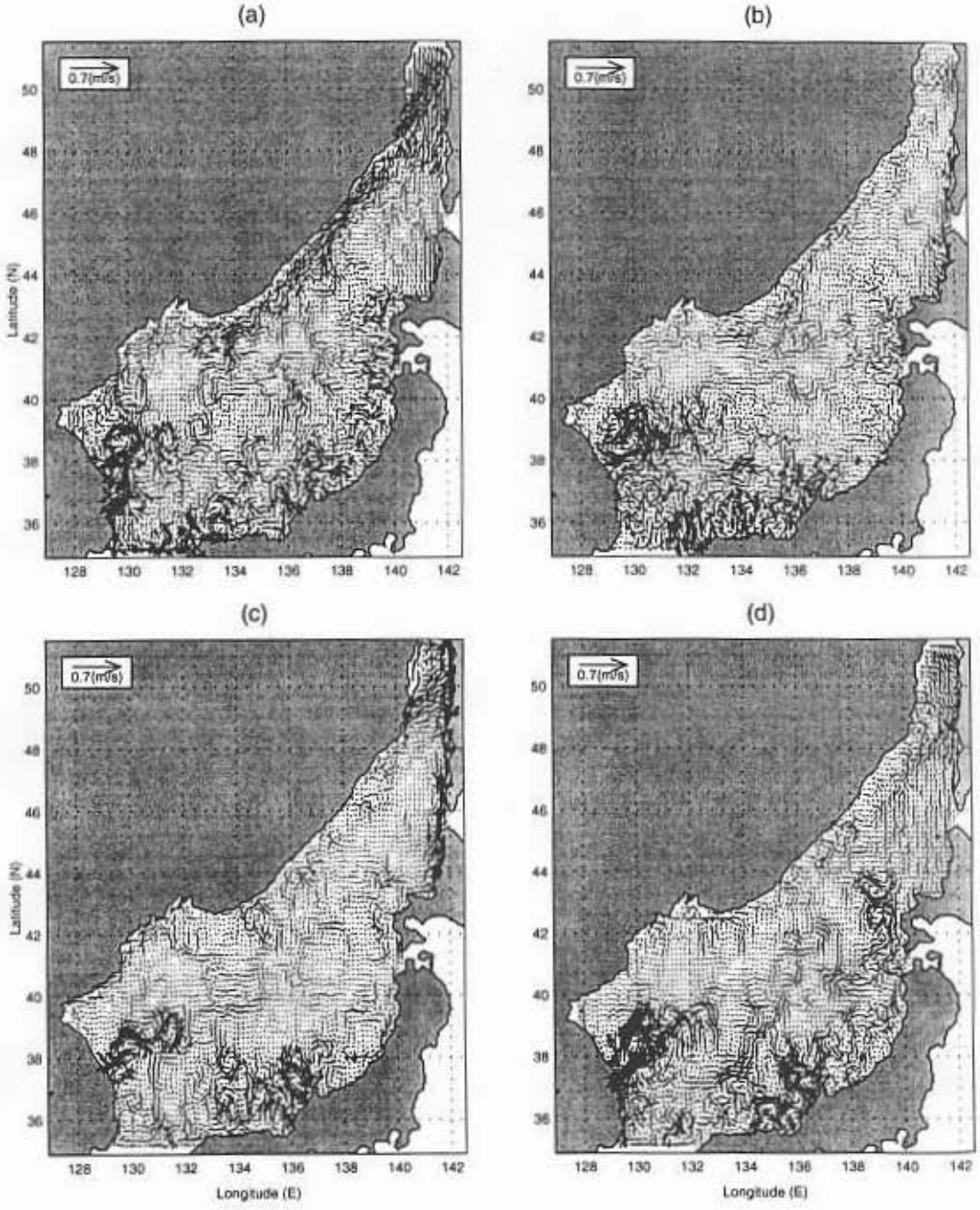

Fig. 8. Surface circulation driven by the winds: (a) January, (b) April, (c) July and (d) October.

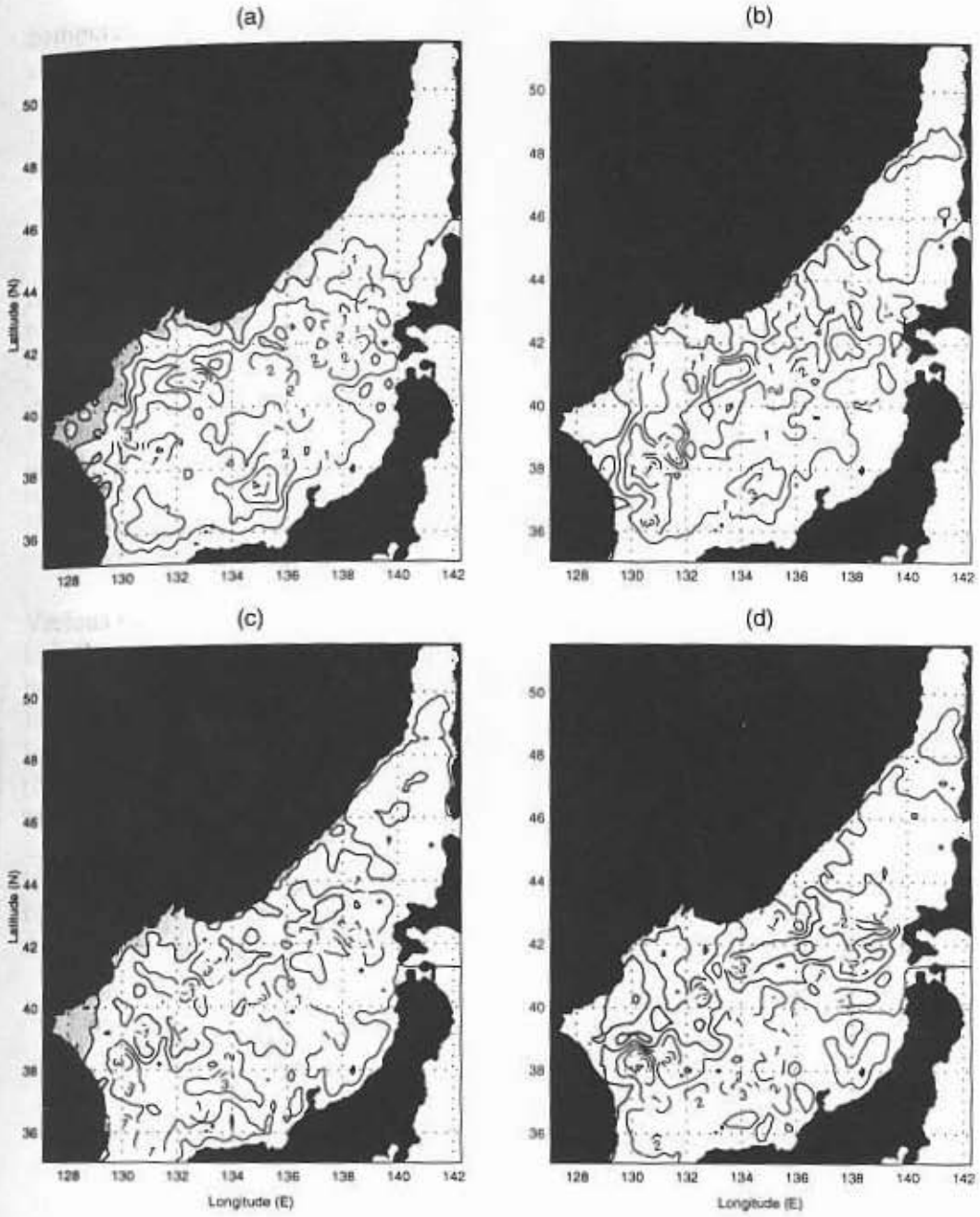

Fig. 9. Volume transport driven by the lateral forcing: (a) January, (b) April, (c) July and (d) October.